BULLETIN OF THE POLISH ACADEMY OF SCIENCES
TECHNICAL SCIENCES, Vol. 67, No. 4, 2019
DOI: 10.24425/bpasts.2019.130183

Intelligent multi-agent system for DC microgrid energy coordination control

P. QADERI-BABAN[1], M.B. MENHAJ[2], M. DOSARANIAN-MOGHADAM[1]*, and A. FAKHARIAN[1]

[1] Faculty of Electrical, Biomedical and Mechatronics Engineering, Qazvin Branch, Islamic Azad University, Qazvin, Iran
[2] Department of Electrical Engineering, Amirkabir University of Technology, Tehran, Iran

Abstract. In this paper, an energy coordination control method based on intelligent multi-agent systems (MAS) is proposed for energy management and voltage control of a DC microgrid. The structure of the DC microgrid is designed to realize the mathematical modeling of photovoltaic cells, fuel cells and batteries. A two-layer intelligent MAS is designed for energy coordination control: grid-connection and islanding of a DC microgrid is combined with energy management of PV cells, fuel cells, loads and batteries. In the hidden layer and the output layer of the proposed neural network there are 17 and 8 neurons, respectively, and the "logsig" activation function is used for the neurons in the network. Eight kinds of feature quantities and 13 different actions are taken as the input and output parameters of the neural network from the micro-source and the load, and the as the control center agent's decision-makers. The feasibility of the proposed intelligent multi-agent energy coordination control strategy is verified by MATLAB/Simulink simulation, and three types of examples are analyzed after increasing the load. The simulation results show that the proposed scheme exhibits better performance than the traditional approaches.

Key words: multi-agent system, DC microgrid, energy management, coordinated control, voltage control.

1. Introduction

The concept of a microgrid (MG) has been gaining attention as a key piece of the puzzle in the evolution towards a reduced carbon footprint and the development of the smart grid. By creating smaller networks, typically at low or medium voltages (LV, MV), MGs can utilize the waste heat from distributed generation (DG) sources for space heating and cooling as well as for industrial processes. These combined heat and power (CHP) systems greatly improve energy efficiency and therefore reduce emissions. Also, MGs aim to integrate renewable energy sources (RES) along with energy storage systems (ESS) to further reduce their CO_2 emissions, and to help meet environmental mandates [1, 2]. Droop control has been proposed as the best solution for decentralized primary control of inverter-based MGs, as they can emulate virtual inertia. Voltage source inverters (VSI) with droop control, which can subsequently be adjusted through secondary control after each imbalance event, have been proposed [3]. A similar droop control method for primary control is explained and implemented along with a decentralized MAS for secondary and tertiary control. They will be described next. MAS is the focus of many ongoing studies as it presents a very flexible and robust framework for distributed systems [4, 5]. In an MAS, each agent is intelligent and independent and has the ability to communicate and cooperate with other agents for a common goal. For MGs, this concept introduces an exciting possibility of having a reliable and adaptable electrical network able to grow and evolve without the need for much infrastructure and centralized control. In this work, an MAS is implemented where each DG, ESS and load feeder is represented by an agent that communicates only with the adjacent agents, yet they all seek a global objective.

The latest literature in terms of MG resource optimization includes [11], where the authors implement optimal power flow (OPF), taking account of system constraints, and Local Controllers are coordinated with the microgrid central controller to reach each resource's optimal power point. In [12], model predictive control, which uses support vector machines to forecast RES output and load levels, is combined with mixed integer linear programming to minimize MG operating costs. A multi-objective genetic algorithm using high temporal resolution insolation data is used to find the optimal design of a DC MG in [13]. These optimization methods so far depend on a central controller and are thus vulnerable to the single point of failure (SPOF) factor and the curse of dimensionality problems given the complicated communication infrastructure and high computational demand of the central entity as more elements are added to the MG. Considering tertiary control, in [14], a droop controlled DC MG is optimized by an MAS using the dynamic consensus algorithm, though only the global efficiency of the converters is considered. A similar but modified consensus algorithm is used in [15] for optimal resource management in an MG, but primary control is not detailed. Another revision on the consensus algorithm is used in [16] along with multistep optimization which considers ESS for EA, yet primary control is ignored again.

*e-mail: m_dmoghadam@qiau.ac.ir

Manuscript submitted 2018-07-20, revised 2018-11-13, initially accepted for publication 2018-11-21, published in August 2019

In this paper, a two-layer multi-agent control system is proposed for a DC microgrid, in which the upper layer is the control center agent and the lower layer includes a photovoltaic cell agent, fuel cell agent, load agent and battery agent. After that, an 8-input 8-output neural network, as a control center agent decision-maker, can output 13 types of control commands to achieve the management of a microgrid. Our contributions are to propose a novel intelligent scheme for DC microgrid energy management that can achieve coordinated control of the microgrid and load, and maintain stability of the DC bus voltage.

The remainder of this paper is organized as follows. In Section 2, a DC microgrid model is introduced. Section 3 presents our proposed control method. Section 4 provides description of case studies. And finally, in Section 5, conclusions are presented.

2. DC microgrid model

As shown in Fig. 1, the structure of the DC microgrid constructed in this paper is composed of a photovoltaic cell, a fuel cell, a battery, a DC load and an AC load. It is connected to the grid through a DC/AC inverter and can be run in parallel. The DC bus voltage rating is set to 350 V [17]. The load is divided into primary load, secondary load and tertiary load according to the degree of importance. Among them, the primary load can be a source of AC, the secondary load can provide short time power and the tertiary load can provide long time power.

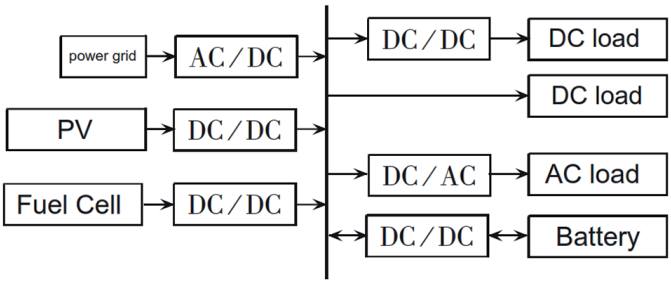

Fig. 1. Structure of DC microgrid

2.1. Photovoltaic cell modeling. The mathematical model of photovoltaic cells is shown as [18]:

$$\mathbf{I_{PV}} = \mathbf{I_{SC}}\left[1 - C_1\left(e^{\frac{\mathbf{U_{PV}} - \mathbf{D_U}}{C_2\mathbf{U_{OC}}}}\right)\right] + \mathbf{D_I} \tag{1}$$

where $\mathbf{I_{SC}}$ is the short-circuit current and $\mathbf{U_{OC}}$ is open-circuit voltage. Also in (1), $\mathbf{U_{PV}}$ and $\mathbf{I_{PV}}$ are the output voltage and current, respectively. In addition, in (1) the remaining parameters for the correlation coefficient can be calculated using the following equations:

$$C_1 = \left(1 - \mathbf{I_m}/\mathbf{I_{SC}}\right)e^{-\frac{\mathbf{U_m} - \mathbf{D_U}}{C_2\mathbf{U_{OC}}}} \tag{2}$$

$$C_2 = \left(\mathbf{U_m}/\mathbf{U_{OC}} - 1\right)/\mathbf{In}\left(1 - \mathbf{I_m}/\mathbf{I_{SC}}\right) \tag{3}$$

$$\mathbf{D_I} = \boldsymbol{\alpha}\left(\mathbf{R}/\mathbf{R_{ref}}\right)\mathbf{D_T} + \left(\mathbf{R}/\mathbf{R_{ref}} - 1\right)\mathbf{I_{SC}} \tag{4}$$

$$\mathbf{D_U} = -\boldsymbol{\beta}\mathbf{D_T} - \mathbf{R_S}\mathbf{D_I} \tag{5}$$

$$\mathbf{D_T} = \mathbf{T_C} - \mathbf{T_{ref}} \tag{6}$$

where $\mathbf{I_m}$ and $\mathbf{U_m}$ are the maximum power point current and voltage, respectively. Also, $\mathbf{R_{ref}}$ and $\mathbf{T_{ref}}$ are the irradiance intensity and the reference value of the photovoltaic cell temperature, respectively. In addition, $\mathbf{R_S}$ is the resistance of photovoltaic cells, $\mathbf{T_C}$ is photovoltaic cell temperature, $\mathbf{R}$ is irradiance intensity, and $\boldsymbol{\alpha}$ and $\boldsymbol{\beta}$ refer to the sunshine current and voltage change temperature coefficient, respectively.

2.2. Fuel cell modeling. The mathematical model of a fuel cell is described as [19]:

$$\mathbf{U_{FC}} = \mathbf{E_{FC}} - \mathbf{U_{act}} - \mathbf{U_{con}} - \mathbf{U_{ohm}} \tag{7}$$

where $\mathbf{U_{FC}}$ is the fuel cell output voltage, $\mathbf{U_{act}}$ is the thermodynamic electromotive force for fuel cells, $\mathbf{U_{con}}$ is the concentration of polarization loss potential, and $\mathbf{U_{ohm}}$ is ohmic polarization loss potential. The corresponding formula is presented as:

$$\mathbf{E_{FC}} = \mathbf{N_0}\left[\mathbf{E_{FC0}} + \frac{\mathbf{R_{FC}}\mathbf{T_{FC}}}{2\mathrm{F}}\,\mathbf{In}\,\frac{\mathbf{P_{H^2}}\mathbf{P_{O^2}^{1/2}}}{\mathbf{P_{H^2O}}} + \mathbf{In}\,\mathbf{P}\right] \tag{8}$$

$$\mathbf{U_{act}} = \mathbf{a} + \mathbf{b}\,\mathbf{lg}\mathbf{i_{FC}} \tag{9}$$

$$\mathbf{U_{act}} = -\frac{\mathbf{R_{FC}}\mathbf{T_{FC}}}{2\mathrm{F}}\,\mathbf{In}\left(1 - \frac{\mathbf{i_{FC}}}{\mathbf{i_{FCL}}}\right) \tag{10}$$

$$\mathbf{U_{ohm}} = -0.126\,\mathbf{I_{FC}}\,e^{-2870\left(\frac{1}{1273} - \frac{1}{\mathbf{T_{FC}}}\right)} \tag{11}$$

where $\mathbf{N_0}$ is the number of batteries in a series, $\mathbf{E_{FC0}}$ is open-circuit voltage and $\mathbf{R_{FC}}$ is the universal gas constant. Also, $\mathbf{P_{H^2}}$, $\mathbf{P_{O^2}}$, $\mathbf{P_{H^2O}}$ are the hydrogen, oxygen and water vapor pressures, respectively. In addition, $\mathbf{P}$ is the battery stack system pressure, $\mathbf{a}$, $\mathbf{b}$ are thermodynamic constants, and $\mathbf{I_{FC}}$ is the battery stack current.

2.3. Battery modeling. The mathematical model of the battery is shown as:

$$\mathbf{U_{bat}} = \mathbf{U_{bat0}} + \mathbf{E_{dyn}} + \mathbf{E_{NL}} + \mathbf{E_{xp}} - \mathbf{i_{bat}}\mathbf{R_{bat}} \tag{12}$$

where $\mathbf{U_{bat}}$, $\mathbf{U_{bat0}}$, $\mathbf{i_{bat}}$, $\mathbf{R_{bat}}$ are the battery output voltage, open circuit voltage, discharge current and internal resistance, respectively. In addition, $\mathbf{E_{dyn}}$ is the concentration of polariza-

tion voltage, and $\mathbf{E_{NL}}$ is active polarization voltage. Also, $\mathbf{E_{xp}}$ is used to fit the battery charge and discharge process to the index change process. The corresponding formula is shown as:

$$\mathbf{E_{dyn}} = \begin{cases} -\mathbf{K}\dfrac{\mathbf{Q}}{\mathbf{Q}-\int \mathbf{i_{bat}}\mathbf{dt}}\mathbf{i_{bat}} & \text{when discharging } (\mathbf{i_{bat}} > 0) \\ -\mathbf{K}\dfrac{\mathbf{Q}}{0.1\mathbf{Q}+\int \mathbf{i_{bat}}\mathbf{dt}}\mathbf{i_{bat}} & \text{when charging } (\mathbf{i_{bat}} < 0) \end{cases} \tag{13}$$

$$\mathbf{E_{NL}} = -\mathbf{K}\frac{\mathbf{Q}}{\mathbf{Q}-\int \mathbf{i_{bat}}\mathbf{dt}}\int \mathbf{i_{bat}}\mathbf{dt} \tag{14}$$

$$\mathbf{E_{xp}} = \mathbf{L}^{-1}\left[\frac{\mathbf{A}}{\left[1/(\mathbf{B}|\mathbf{i_{bat}}|)\right]\mathbf{s}+1} + \mathbf{s_{bat}}\right] \tag{15}$$

where **K** is the polarization voltage, **Q** is battery capacity, **A** and **B** are the exponential curve of peak voltage and inverse of the time constant, respectively. Also, in (15) the working state of the battery is calculated using the following equation:

$$\mathbf{s_{bat}} = \begin{cases} 0 & \text{when discharging } (\mathbf{i_{bat}} > 0) \\ 1 & \text{when charging } (\mathbf{i_{bat}} < 0). \end{cases} \tag{16}$$

3. MAS

3.1. Applicability of MAS. The MAS can improve the ability of the computer system to solve complex problems by simulating the operation mechanism of the human social system. In this scheme, the large and complex system is divided into a number of agents. Each agent can perform different tasks separately, and can solve complex problems that cannot be solved by a single agent through coordination and cooperation. This scheme is suitable for decentralized and complex control of microgrids.

a. Autonomy: agents have the ability to control themselves. In the absence of external interference, agents can control themselves to accomplish certain tasks according to their own situation.
b. Collaboration: agents can communicate with each other. An agent can send its own state to other agents, and coordinates itself with other agents to complete a certain task.
c. Reactivity: agents can get information from the environment or from other agents. They can provide a reasonable response based on the information obtained, and change their own state.

3.2. Proposed MAS structure. The proposed energy control system based on the multi-agent approach is shown in Fig. 2. In this system, the upper control center agent is used to collect the information from each agent, and to develop a reasonable policy, while the policy is distributed down to the lower agent.

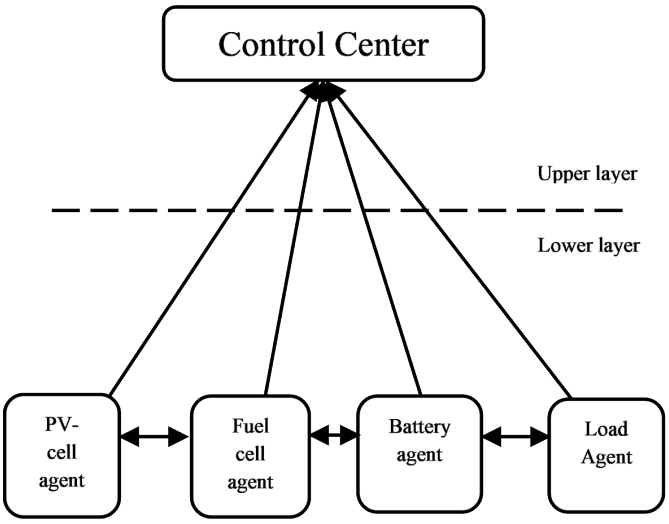

Fig. 2. Structure of MAS

In addition, the control center agent also controls the straight grid and the network. The lower agent consists of PV cells, fuel cells, batteries and four sub-agent loads. Each child agent uploads its own operating parameters to the control center agent. According to the agent's downloaded plan and its own conditions, the status of the operation will be decided by the control center agent. At the same time, the lower agent has the following different functions:

a. PV cell agent has the maximum power point tracking (MPPT) function so that the PV can generate maximum power but also has the ability to decide whether to access the microgrid;
b. The fuel cell agent has the function of monitoring the running status and determining whether to access the microgrid;
c. The battery agent monitors the voltage, the remaining capacity and other operating parameters, and has the function of determining the battery charge and discharge. It is decided in this paper that when the state of charge (SoC) is less than 20%, then discharge is not allowed, and when the SoC is higher than 90%, charge is not allowed;
d. The load agent can calculate the current's total load power and can decide to reduce the load according to the total power of the distributed power supply and the total load power, and at the same time reasonable load shedding can be carried out based on the importance of the load.

3.3. Neural network algorithm. Artificial neural networks (ANN) are a new information-processing and computing technique inspired by biological neuron processing. ANN models have been widely applied in various fields of science and technology involving time series forecasting, pattern recognition and process control [20]. Therefore, this paper chooses the neural network as the decision-maker of the control center agent.

In this paper, the proposed neural network is used to achieve the following objectives: first, the PV battery works in the MPPT mode, while the DC/DC converter regulates the output voltage. When the maximum output of photovoltaic cells is greater than

the load power, if the battery allows charging, it will generate additional energy stored in the battery. Otherwise, the PV battery is not sufficient to reach the constant voltage output. When the photovoltaic cell is insufficient to provide enough energy, the fuel cell can be discharged. Deciding whether to discharge the fuel cell is based on whether the power balance condition is satisfied or not. Afterwards, if the photovoltaic cells, fuel cells and batteries cannot meet the power requirements, depending on the power, the grid can provide power to the network or decide on load shedding. Therefore, the proposed neural network can control the system to make full use of the renewable distributed power supply, reduce the output of the large power grid as much as possible, and minimize the consumption of fossil energy and the expenditure of electricity based on ensuring the normal power consumption of users.

To achieve the above objectives, first construct a 2-layer back propagation (BP) neural network whose structure is shown in Fig. 3, where, **P**, **T** stand for the input and output data, $\mathbf{W}_{\mathrm{I}}^{1,1}$, $\mathbf{W}_{\mathrm{L}}^{1,2}$ is the weight matrix, $\mathbf{b}^{1}$, $\mathbf{b}^{2}$ stand for the threshold, hidden layer and output layer of 17 and 8 neurons, respectively, and the transfer function uses logsig (·). The input layer and output layer data of the neural network are shown in Table 1 and Table 2, respectively. The input layer consists of eight characteristic parameters which are uploaded by the lower layers, including the operation status of the photovoltaic cells, fuel cells, batteries, power grids and loads. The output of the output layer consists of 13 outputs, representing 13 coordinate control commands to control fuel cells, batteries, power grids and loads. Table 3 corresponds to the 13 coordinated control commands. Finally, a 10 000 group-strong training sample is generated randomly to complete the training network and generate the Simulink module.

Table 1
Characteristic parameters at input layer

Element	Characteristic Parameters	Eigenvalues	Description
PV	Maximum output power	P_{mP}	–
Fuel cell	Whether to allow discharge	1 0	Allow discharge Prohibit discharge
	Maximum output power P	P_{mf}	–
Battery	Whether to allow discharge	1 0	Allow discharge Disables discharge
	Whether to allow charging	1 0	Allow charging No charge is allowed
	Maximum output power	P_{mb}	–
Power grid	Whether to allow discharge	1 0	Allow discharge Prohibit discharge
Load	Load power	P_{L}	–

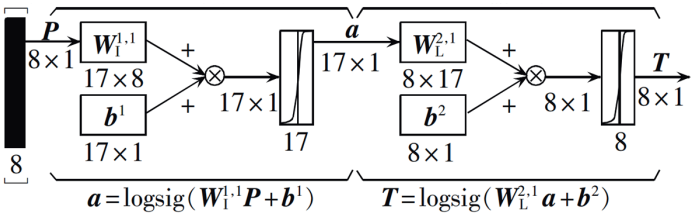

Fig. 3. Structure of BP neural network

Table 2
Output layer characteristic parameters

Element	Characteristic Parameters	Eigenvalues	Description
PV	Discharge situation	0	MPPT mode constant voltage output
		1	Non-MPPT mode constant voltage output
Fuel cell	Discharge situation	1.0	Constant pressure discharge
		0.0	Not discharge
		0.1	Maximum power discharge
Battery	Discharge situation	1.0	Constant pressure discharge
		0.0	Not discharge
		0.1	Maximum power discharge
	Whether to charge	1	Charge
		0	Not charged
Power grid	Whether to allow discharge	1	Discharge
		0	Not discharge
Load	Whether the load shedding	1	Load shedding
		0	Not overloaded

Table 3
Outputs of energy coordination control

PV battery discharge situation	Fuel cell discharge situation		Battery			Whether the grid is discharged	Whether the load is reduced
			Discharge situation		Whether to charge		
1	0	0	0	0	0	0	0
0	0	0	0	0	1	0	0
0	1	0	0	0	0	0	0
0	0	1	1	0	0	0	0
0	0	0	0	1	0	1	0
0	0	1	0	1	0	0	1
0	0	1	0	0	0	1	0
0	0	1	0	0	0	0	1
0	0	0	1	0	0	0	0
0	0	0	0	1	0	0	1
0	0	0	0	1	0	1	0
0	0	0	0	0	0	1	0
0	0	0	0	0	0	0	1

4. Case study

The simulation system includes one of the photovoltaic cells, the fuel cells and batteries. Among them, the maximum output power of the fuel cell and the battery is 2 kW and 2.5 kW, respectively, and the initial SoC of the battery is 50%. There are also four types of loads in the system: large power grid and 1 kW first class, 2 kW first class, 2 kW second class, and 2 kW third class.

4.1. Example 1. Load to keep 1 kW unchanged, when the irradiance as shown in Fig. 4a changes. The DC bus voltage shown in Fig. 4b while changes in load power $\mathbf{P_L}$, photovoltaic cell power $\mathbf{P_{PV}}$, fuel cell power $\mathbf{P_{FC}}$, battery power $\mathbf{P_{bat}}$ and grid power $\mathbf{P_{Grid}}$ are shown in Fig. 5. Among them, $\mathbf{P_{bat}}$ is negative while, $\mathbf{P_{PV}}$, $\mathbf{P_L}$, $\mathbf{P_{FC}}$ and $\mathbf{P_{Grid}}$ are positive.

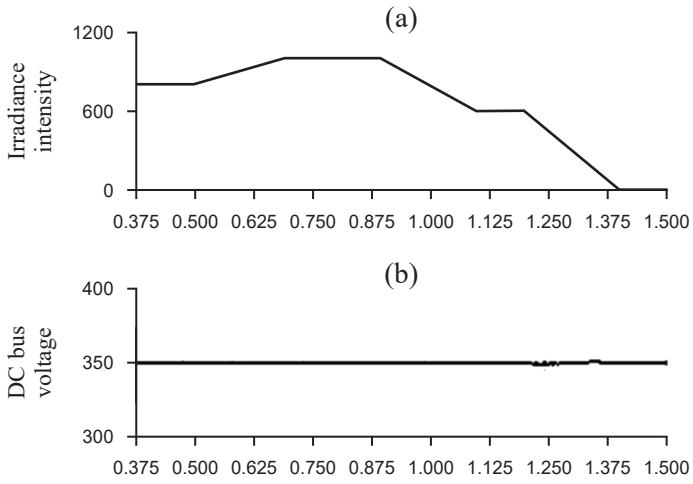

Fig. 4. Irradiance intensity (a) and voltage of DC bus (b)

Initial irradiance intensity is 800. The maximum output power of a photovoltaic cell is about 1250 W, which ensures a normal load of 1 kW. At the same time, because the initial SoC of the battery is 50%, to meet the charging requirements, the battery agent allows the battery to charge. The control center agent receives the battery to allow charging information, issued as (0, 0, 0, 0, 0, 0, 0) with the battery charge of 0.5 ∼ 0.9 s. The irradiance intensity gradually increases to 1000 W/m^2 and remains unchanged, the maximum output of the PV is also increased [(0, 0, 0, 0, 0, 1, 0, 0) command] and the battery maintains the state of charge while the charging power gradually increases to 580 W and remains unchanged (0.9 ∼ 1.2 s). Irradiance intensity gradually weakens to 600 W/m^2 and remains the same, at its most photovoltaic. The output is reduced to 940 W, of which at 1.08 s, the maximum output of the PV is 1000 W, then in the course of 0.9 ∼ 1.08 s, the control center agent is still issued (0, 0, 0, 0, 0, 1, 0, 0), and in the course of 1.08 ∼ 1.2 s, the PV cell cannot meet the load demand. Since the fuel cell is allowed to discharge and the maximum total output power of the PV can meet the load requirements, the control center agent sends out (0, 1, 0, 0, 0, 0, 0, 0), the battery stops charging and the fuel cell starts constant voltage discharge. After 1.2 s, the PV output decreases as illumination decreases, and the control center agent still sends the (0, 1, 0, 0, 0, 0, 0, 0) command, the fuel cell continues the constant voltage discharge, and output power gradually increases.

4.2. Example 2. Initially, the microgrid is operated in parallel with the primary load of 1 kW, 0.5 s, 0.75 s and 1 s, respectively. For each 2 kW, the large power grid at 1.25 s when the open micro-network is put into the island running state. The corresponding power change is shown in Fig. 6. At the

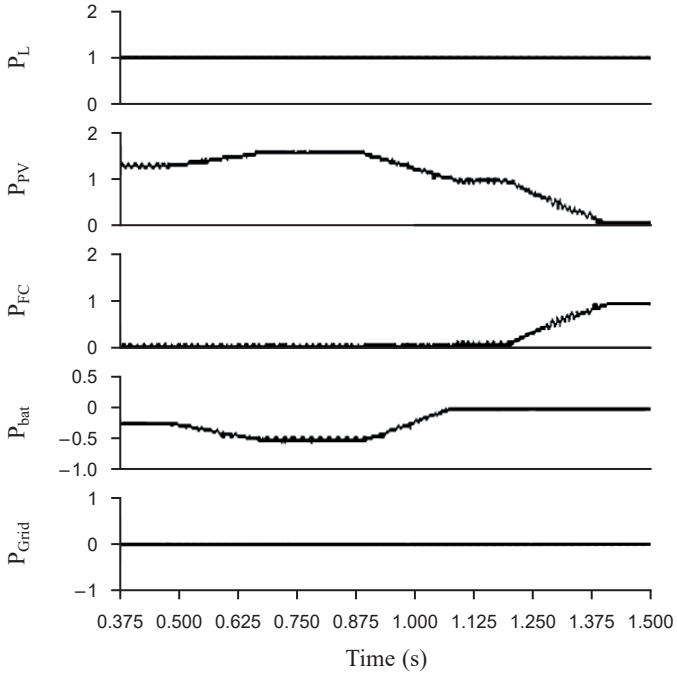

Fig. 5. Results of energy coordination control in case 1

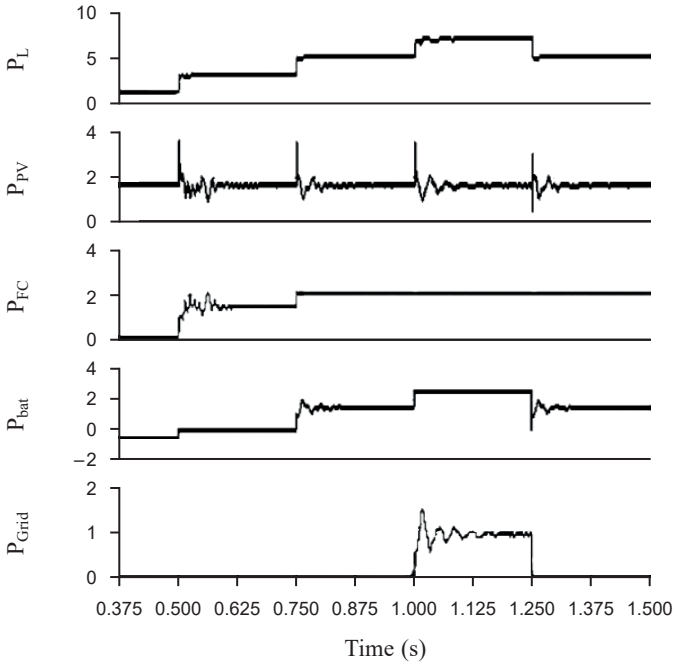

Fig. 6. Results of energy coordination control in case 2

beginning, the maximum output power of the PV is about 1.58 kW, and there is only 1 kW load in the system. Since the battery agent is 50%, the battery agent allows the battery to be charged, and the control center agent sends out the information (0, 0, 0, 0, 1, 0, 0), and then the battery is charged. An additional 2 kW secondary load is added at 0.5 s, the PV is insufficient to provide the required power, and the power supply will be provided by other power supplies. At this point, the fuel cell allows for discharge and the maximum total output with the PV (0, 1, 0, 0, 0, 0, 0) control tasks, for the battery to stop charging and allow the fuel cell for constant voltage discharge. A 0.75 s increase is noted for the power consumption, and with 2 kW three-stage load, photovoltaic and fuel cells cannot meet the load requirements, but the battery SoC allows for its discharge and the photovoltaic, fuel cell and battery maximum output power of 6.08 kW meets the load requirements. The control center agent issues the (0, 0, 1, 1, 0, 0, 0, 0) command, and the maximum power of the fuel cell discharge and battery constant voltage discharge are attained after 1 s, when following the increase in the 2 kW load, photovoltaic, fuel cells and batteries cannot meet the load requirements. The control center will then issue the (0, 0, 1, 0, 1, 0, 1, 0) command, the maximum power of the fuel cell and the battery discharge will be attained and the large grid shall begin to provide power to the micro-network (1.25 s, large power grid. At this point, the system micro-source power cannot meet the load and the control center issues the (0, 0, 1, 0, 1, 0, 0, 1) command, i.e. load shedding. After receiving the load shedding information, the load agent will select a reasonable load shedding method according to the sum of the maximum output power obtained from the photovoltaic cell agent, fuel cell agent and battery agent. In this example, the load agent chooses to disconnect the 2 kW three-stage load, and the corresponding load input and load shedding are shown in Fig. 7. After the load shedding is completed, the control center agent issues the (0, 0, 1, 1, 0, 0, 0, 0) command again, demanding the maximum power discharge of the fuel cell and the constant voltage discharge of the battery. The corresponding DC bus voltage is shown in Fig. 8. It can be seen that the energy coordination control can recover more effectively and maintain the DC bus voltage at about 350 V.

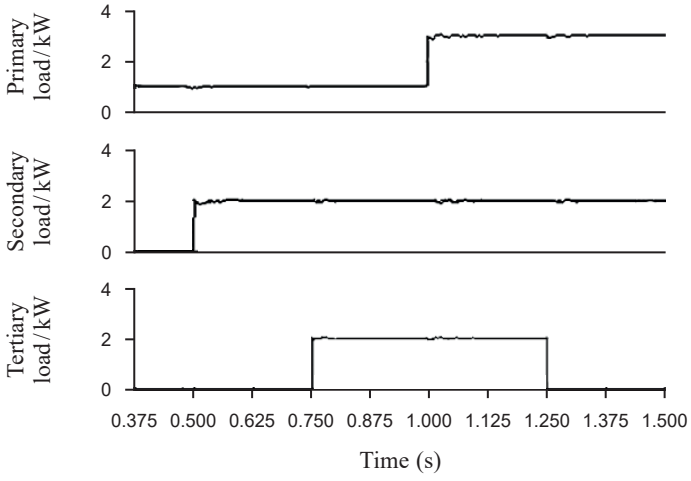

Fig. 7. Results of load control by load Agent in case 1

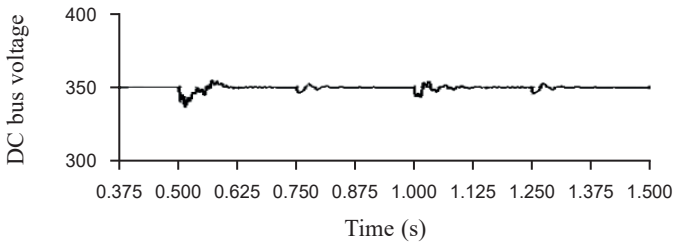

Fig. 8. Voltage of DC bus

4.3. Example 3. During initial microgrid island operation is performed at a load of 1 kW, and when the load is 2 kW and 1.25 s, the microgrid is connected with the large power grid and enters the grid running status. The power change is shown in Fig. 9. The rate can meet the load requirements, and the energy coordination control decision is the same as the case of the first 1 s of Example 2. At 1 s, a 2 kW primary load is added, because the large power grid does not allow discharge at this time, and the photovoltaic cells, fuel cells and batteries are insufficient to provide the required power. The control center sends (0, 0, 1, 0, 1, 0, 0, 1), notifying the load agent to commence load shedding. After the load agent receives the load shedding information, it is decided to connect the 2 kW primary load at the same time, disconnect the 2 kW tertiary load, and ensure that the voltage is stable while keeping critical loads running. After disconnecting the three-stage load, the control center agent will issue the (0, 0, 1, 1, 0, 0, 0, 0) command. At 1.25 s, the

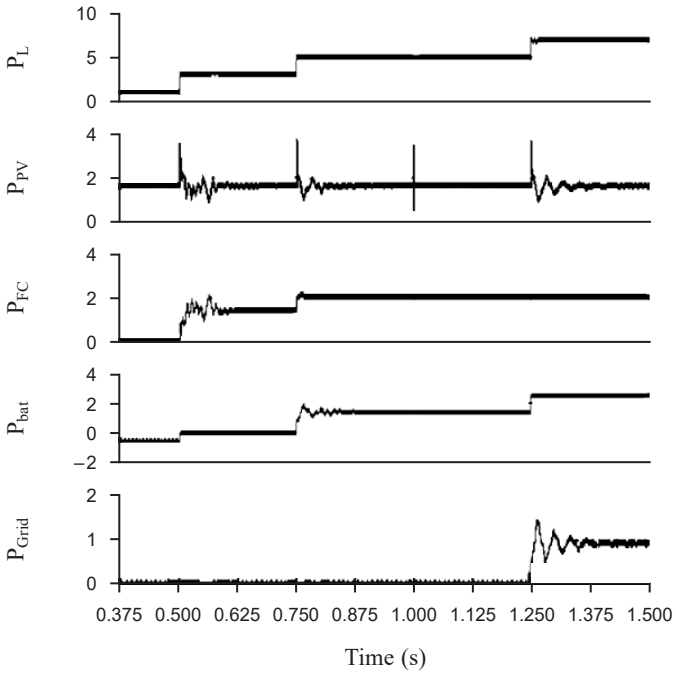

Fig. 9. Results of energy coordination control in case 3

microgrid is connected to the grid and the load agent confirms that the large grid can supply power to the microgrid. When the three-stage load will be disconnected before reconnecting, the control center agent will issue the (0, 0, 1, 0, 1, 0, 1, 0) command, and then discharge the maximum power of the battery and power grid supplies power to the microgrid to guarantee power balance and maintain voltage stability. The corresponding load changes and DC bus voltage are shown in Fig. 10 and Fig. 11, respectively.

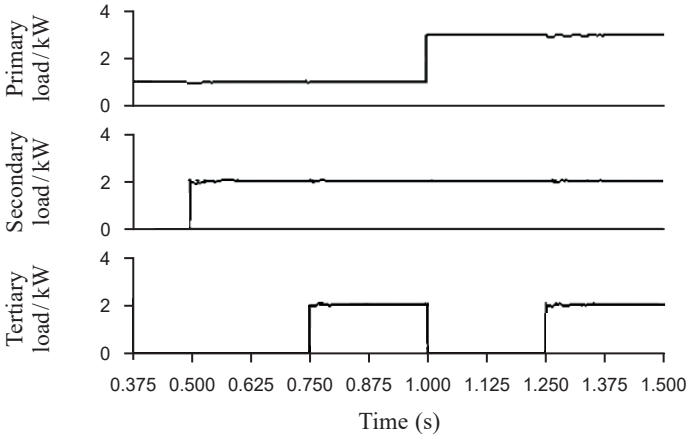

Fig. 10. Results of load control by load Agent in case 2

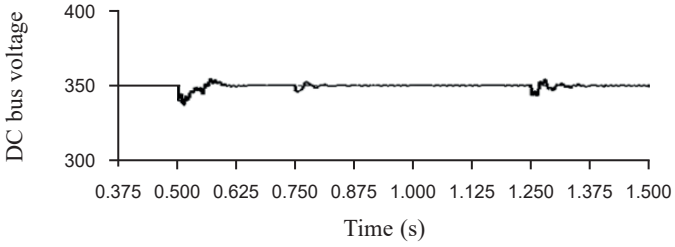

Fig. 11. Voltage of DC bus

In this study, the performance of the new multi-agent based on ANN architecture has been compared to a conventional centralized energy management system (EMS). The centralized EMS was built based on the typical centralized control topology as in [21]. All constraints as in the distributed controller were implemented in the centralized controller, and all calculations were performed by a single centralized controller. In order to perform the comparison, both systems were simulated based on the same input parameters and disturbances. The ANN performances were evaluated based on efficiency parameters and power losses, and the results for each example (Ex. 1, Ex. 2 and Ex. 3) are listed in Table 4.

It is noticeable from the results that the centralized method has lower efficiency for each parameter as compared to the multi-agent based on ANN. This is because the MAS based on ANN consists of agents that are distinct and unique to the different types of energy sources and also distinct individually according to capacity, size and control algorithm. Therefore, it

Table 4
Outputs of energy coordination control

methods	Multi-agent based ANN			Centralized		
	Ex. 1	Ex. 2	Ex. 3	Ex. 1	Ex. 2	Ex. 3
η_{sys}	0.771	0.753	0.684	0.639	0.603	0.54
η_{PV}	0.853	0.772	0.612	0.677	0.621	0.517
η_{FC}	0.885	0.813	0.673	0.653	0.643	0.533
η_{bat}	0.856	0.828	0.654	0.687	0.668	0.526
P_{Loss} (%)	1.211	2.039	3.634	2.541	4.037	7.636

can provide faster control than the corrective approach of conventional centralized control. The lower efficiency of the centralized method also contributed to the computational burden of the centralized controller due to the extensive computation for performing optimization that later caused slow reaction time in handling the changes and disturbances that occurred in the microgrid.

5. Conclusions

In this paper, we proposed an intelligent microgrid control system based on intelligent MAS. It mainly has the following characteristics:

a. The lower level of all agents can run according to their own situation; however, to cooperate with each other, they make full use of the agent's autonomy and collaboration;
b. The upper control center agent sees the neural network as the decision-maker, and can thus provide reasonable responses according to the information uploaded by the lower agent, realize the hierarchical control and ensure a reasonable flow of energy;
c. Through the MAS, in the event of increased load, island and grid state transition, etc., the stability of the DC bus voltage can be maintained effectively.

While this study was carried out in MATLAB, an interesting line of investigation could be to implement MAS using the JADE platform in-depth studies to yield further fruitful results.

References

[1] N. Hatziargyriou, H. Asano, R. Iravani, and C. Marnay, "Microgrids," *IEEE Power and Energy Magazine*, 5(4) 78–94, July–August 2007.
[2] P. Komarnicki, "Energy Storage Systems: Power Grid and Energy Market Use Cases," *Archives of Electrical Engineering*, *Journal of PAS*, 65(3) 495–511, Sep. 2016.
[3] D. Gao, J. Jiang, and S. Qiao, "Comparing the Use of Two Kinds of Droop Control Under Microgrid Islanded Operation Mode," *Archives of Electrical Engineering*, *Journal of PAS*, 62(2) 321–331, Jun. 2013.
[4] R. Olfati-Saber, J.A. Fax, and R. M. Murray, "Consensus and Cooperation in Networked Multi-Agent Systems," *Proceedings of the IEEE*, 95(1) 215–233, Jan. 2007.

[5] A.H. Sayed, "Adaptive Networks," *Proceedings of the IEEE*, 102(4) 460–497, Apr. 2014.
[6] J. Chen and A.H. Sayed, "Diffusion Adaptation Strategies for Distributed Optimization and Learning Over Networks," *IEEE Transactions on Signal Processing*, 60(8) 4289–4305, Aug. 2012.
[7] J. Chen and A. H. Sayed, "Distributed Pareto Optimization via Diffusion Strategies," *IEEE Journal of Selected Topics in Signal Processing*, 7(2) 205–220, Apr. 2013.
[8] S.-Y. Tu and A. H. Sayed, "On the Influence of Informed Agents on Learning and Adaptation Over Networks," *IEEE Transactions on Signal Processing*, 61(6) 1339–1356, Mar. 2013.
[9] V. Salehi, A. Mohamed, A. Mazloomzadeh, and O. A. Mohammed, "Laboratory-Based Smart Power System, Part I: Design and System Development," *IEEE Transactions on Smart Grid*, 3(3) 1394–1404, Sept. 2012.
[10] V. Salehi, A. Mohamed, A. Mazloomzadeh, and O.A. Mohammed, "Laboratory-Based Smart Power System, Part II: Control, Monitoring, and Protection," *IEEE Transactions on Smart Grid*, 3(3) 1405–1417, Sept. 2012.
[11] W. Shi, X. Xie, C.-C. Chu, and R. Gadh, "Distributed Optimal Energy Management in Microgrids," *IEEE Transactions on Smart Grid*, 6(3) 1137–1146, May 2015.
[12] A. Parisio, E. Rikos, and L. Glielmo, "A Model Predictive Control Approach to Microgrid Operation Optimization," *IEEE Transactions on Control Systems Technology*, 22(5) 1813–1827, Sept. 2014.
[13] M.B. Shadmand and R.S. Balog, "Multi-Objective Optimization and Design of Photovoltaic-Wind Hybrid System for Community Smart DC Microgrid," *IEEE Transactions on Smart Grid*, 5(5) 2635–2643, Sept. 2014.
[14] L. Meng, T. Dragicevic, J.M. Guerrero, and J.C. Vasquez, "Dynamic Consensus Algorithm based Distributed Global Efficiency Optimization of a Droop Controlled DC Microgrid," *IEEE International Energy Conference (ENERGYCON)* pp. 1276–1283, 13–16 May 2014.
[15] Y. Xu and Z. Li, "Distributed Optimal Resource Management based on the Consensus Algorithm in a Microgrid," *IEEE Transactions on Industrial Electronics*, 62(4) 2584–2592, Apr. 2015.
[16] G. Hug, S. Kar, and C. Wu, "Consensus + Innovations Approach for Distributed Multiagent Coordination in a Microgrid," *IEEE Transactions on Smart Grid*, 6(4) 1893–1903, July 2015.
[17] W. Chen, A.M. Bazzi, J. Hare, and S. Gupta "Real-Time Integrated Model of a Micro-Grid with Distributed Clean Energy Generators and their Power Electronics," *Applied Power Electronics Conference and Exposition (APEC)*, *IEEE*, 20–24 Mar. 2016.
[18] C.D. Fuentes, C.A. Rojas, H. Renaudineau, S. Kouro, M.A. Perez, and T. Meynard, "Experimental Validation of a Single DC Bus Cascaded H-Bridge Multilevel Inverter for Multistring Photovoltaic Systems," *IEEE Transactions on Industrial Electronics* 64(2) 930–934, Feb. 2017.
[19] L. Valverde, C. Bordons, and F. Rosa, "Integration of Fuel Cell Technologies in Renewable-Energy-Based Microgrids Optimizing Operational Costs and Durability," *IEEE Transactions on Industrial Electronic*, 63(1) 167–177, Jan. 2016.
[20] B. Farzanegan, S.D. Banadaki, and M.-B. Menhaj, "Direct Artificial Neural Network Control of Single Link Flexible Joint," *4th International Conference on Control*, *Instrumentation*, *and Automation (ICCIA)*, *IEEE*, 27–28 Jan. 2016.
[21] M. Elsied, A. Oukaour, H. Gualous, and R. Hassan, "Energy Management and Optimization in Microgrid System based on Green Energy," *Energy*, *Elsevier*, 84(C) 139–151, 2015.